1. RESIDUAL MONTE CARLO TREATMENT OF THE TIME VARIABLE

Another extension and improvement for the HOLO method described in Sec. **??** is the time discretization of the transport equation. We have incorporated the time variable into the ECMC method to improve efficiency over IMC, while still preserving the accuracy of MC integration. The main area of interest is in producing more accurate resolution of radiation wave-fronts in optically thin regions, where particles transport a long distance over a time step. In such regions, the MC integration of the time variable by IMC can produce greater accuracy than an implicit Euler discretization, which can produce artificially fast propagation of radiation in space. A potential application where this accuracy is important is stellar atmosphere calculations. It is noted that no adaptive refinement in time is performed, so maintaining exponential convergence may not be possible. However, we still expect the residual MC formulation of the ECMC method to show improvement in efficiency over standard MC.

In the remainder of this chapter, the inclusion of the time variable into the ECMC trial space is detailed, along with modifications to particle tracking and the ECMC algorithm. The process of sampling, tracking, and tallies particle histories in time is detailed in literature[**?**, **?**, **?**, **?**], but sufficient details are provided in this chapter. Finally, a new temporal closure for the LO equations is given, and results are compared to IMC for accuracy and efficiency.

1.1 Modifications to the HO equations

Inclusion of the time variable t in the trial space used by ECMC allows for no discretization of the transport operator $\mathbf{L}$. The transport operator, applied to the

continuous intensity I, becomes

$$\mathbf{L}I(x,\mu,t) = \frac{1}{c}\frac{\partial I}{\partial t} + \mu\frac{\partial I}{\partial x} + \sigma_t I \tag{1.1}$$

The emission source is still treated with an implicit Euler discretization, which is similar to the approximation made in IMC. The ECMC algorithm specified in Sec. **??** does not need to be modified. However, the residual source and trial-space representation are modified to include t. Each batch is still estimating the error in the current projection estimate $\tilde{I}(x,\mu,t)$, but the time variable must be included in the inversion of the $\mathbf{L}$ operator.

1.1.1 The Doubly-Discontinuous Trial Space in Time

It is necessary to define a new trial space that includes the time variable so that we can explicitly evaluate the residual. The time variable has a similar representation to the LDD trial space used for the spatial variable in Sec. **??**, but the solution is a constant value over the interior of the time step. This step, doubly-discontinuous (SDD) trial space is defined as

$$\tilde{I}(x,\mu,t) = \begin{cases} \tilde{I}^n(x,\mu) & t = t^n \\ \overline{I}(x,\mu) & t \in (t^n, t^{n+1}) \\ \tilde{I}^{n+1}(x,\mu) & t = t^{n+1} \end{cases} \tag{1.2}$$

where we have used $\overline{I}$ to denote the time-averaged LDFE *projection* in x and μ of the intensity over the interior of the time step; the beginning and end of time step projections are denoted $\tilde{I}^n$ and $\tilde{I}^{n+1}$, respectively. An illustration of t for the SDD trial space, over the n-th time step, is depicted in Fig. 1.1. There is a projection error in using the LDFE projection to represent the intensity between time steps. However,

with sufficient noise reduction and mesh resolution, this should be an acceptable error compared to the large statistical noise of standard MC.

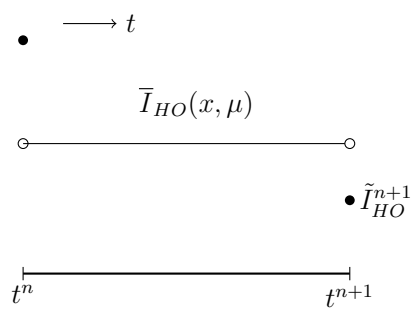

Figure 1.1: Step doubly-discontinuous representation of t for the HO solution.

The SDD trial space provides a projection for all the desired unknowns to exactly produce the moment equations, i.e., the time-averaged, end of time step, and previous time step intensities; temporally, these are the only unknowns that appear in equations that have been integrated over a time step to produce a balance statement. Another benefit of this trial space is it allows for infrastructure for computing the residual from the time-discrete case to be used directly. This trial space has one major drawback: only particle histories that reach t^{n+1} contribute to the estimation of $\tilde{\epsilon}^{n+1}$, and thus I^{n+1}. This is undesirable in optically thick problems.

REWRITE: Possibly move this to the future work section Alternatively, an LDFE representation could be used in the time variable. The linear representation would produce less noise because all particle tracks contribute to the slope, rather than just those that reach the end of the time step, although it would produce an approximate projection error for the end of time step intensity that is not produced with a discontinuity at the end of the time step. The linear representation in time would also

produce a more accurate reconstruction of the scattering source in time. However, a linear representation requires the sampling algorithm to be significantly modified because the L_1 integral for computing the residual magnitude is now significantly complicated by the tri-linear function. A possible way to sample this source is discussed in Appendix??? for completeness, but it has not been rigorously investigated.

1.1.2 Residual Source Definition and Sampling

The residual is defined as $r = q - \mathbf{L}\tilde{I}(x, \mu, t)$, where

$$q = \left(\sigma_a ac(T_{LO}^{n+1})^4(x) + \sigma_s \overline{\phi}_{LO}\right) \tag{1.3}$$

is a constant in time and provided by the LO solver. We have assumed a constant reconstruction for the scattering source in time. Evaluation of the residual with Eq. (1.2) for I produces a uniform source in time, as well as a δ-function source at the beginning and end of the time step. We write the residual source in terms of three components:

$$r(x, \mu, t) = \overline{r}(x, \mu) + r^n(x, \mu)\delta^+(t - t^n) + r^{n+1}(x, \mu)\delta^-(t - t^{n+1}), \quad t \in [t^n, t^{n+1}] \tag{1.4}$$

We will look at each component individually. The first residual term is a constant in time with representation

$$\overline{r}(x, \mu) = q - \mu \frac{\partial \overline{I}(x, \mu)}{\partial x} - \sigma_t \overline{I}(x, \mu) \tag{1.5}$$

Evaluation of the above function produces both face and volumetric sources, similar to in the discrete case. To sample x and μ from the face and volume distributions, the same rejection procedure can be used as for Eq. (**??**) and detailed in [**?**]. The

time variable can then be sampled uniformly over the time step, i.e., $t = t^n + \eta\Delta t$, where η is a uniform random variable with support $(0, 1)$.

The second source has definition

$$r^n(x,\mu) = -\frac{1}{c}\frac{\partial \overline{I}(x,\mu)}{\partial t}\bigg|_{t=t^n} = -\frac{1}{c}\left(\overline{I}(x,\mu) - \tilde{I}^n(x,\mu)\right) \tag{1.6}$$

This source is a LDFE space and angle volumetric source. The rejection sampling procedure is used to sample x and μ. All particles sampled from this source begin tracking with $t = t^n$.

The final source term is

$$r^{n+1}(x,\mu) = -\frac{1}{c}\frac{\partial \overline{I}(x,\mu)}{\partial t}\bigg|_{t=t^{n+1}} = -\frac{1}{c}\left(\tilde{I}^{n+1}(x,\mu) - \overline{I}(x,\mu)\right). \tag{1.7}$$

The source r^{n+1} can be treated using the same analytic treatment as the outflow face source in the LDD trial space, detailed in Sec. **??**; the source at the end of the time step is never sampled because its contribution to I^{n+1} can be analytically computed. To treat the sources this way, the solution for $\tilde{I}^{n+1}(x,\mu)$ is initialized to the value of $\overline{I}(x,\mu)$ before a batch of particles begins. Then, error particles that reach the end of the time step, referred to as "census" particles, contribute a standard score to the projection $\tilde{I}^{n+1}(x,\mu)$.

With these definitions, it is thus only necessary to sample from two sources. Using composite-rejection sampling [**?**], a discrete probability distribution is sampled to determine which source component to sample, followed by sampling of that component. The algorithm is

1. Sample uniform random number η

2. If $\eta < \|r^n\|_1/(\|r^n\|_1 + \|r^{n+1}\|_1)$:

- Sample from r^n source using rejection sampling
- Sample t uniformly over (t^n, t^{n+1}).

3. Else:

   - Sample from $\overline{r}$ source

All L_1 integrals can be analytically integrated using the same numerics as in the time-discrete case. The systematic sampling algorithm, as described in Sec. **??**, can be applied similarly. However, the choice of source is only make locally over that space-angle element. In that case, the element is chosen systematically, then the choice of r^n or $\overline{r}$ is sampled. REWRITE: Only discuss sampling of systematic case.

1.1.3 Importance Sampling on Interior of Time Step

As an attempt to reduce variance in the estimate of $\tilde{\epsilon}^{n+1}(x, \mu)$, we use important sampling in the time variable. Systematic sampling is still used for determining the cell of interest, and sampling as described above is used to determine which source is sampled, based on the appropriate probabilities described in the previous section. However, when the interior source $\overline{r}(x, \mu)$ is sampled, we use importance sampling for the conditional sampling of the uniform time step. The goal is to ensure that some histories reach the end of the time step. In order to do this, we sample from a modified PDF such that a fraction p_{end} of particles sampled from $\overline{r}(x, \mu)$ are born with $t \in (t^{end}, t^{n+1})$. We define $t^{end} = t^{n+1} - M/(c\sigma_t)$, where M is the desired number of MFP of travel the particle will undergo from the end of the time step (e.g., 2 or 3). The weights of particles sampled from this distribution must be modified to prevent source biasing.

The new PDF to be sampled from is

$$f^*(t) = \begin{cases} \dfrac{1 - p_{end}}{t^{end} - t^n} & 0 < t < t^{end} \\ \dfrac{p_{end}}{t^{n+1} - t^{end}} & t^{end} \leq t < t^{n+1} \\ 0 & \text{elsewhere} \end{cases} \tag{1.8}$$

The original PDF is $f(t) = 1/\Delta t$, for $t \in (t^n, t^{n+1})$. Thus, using the standard procedure for importance sampling[**?**], the starting time t_{start} is sampled from $f^*(t)$, and then weights are multiplied by the factor $f(t_{\text{start}})/f^*(t_{\text{start}})$. This procedure is not perfect in that if a particle is moving from an optically thin to an optically thick region, it is not guaranteed to reach census. However, this case does not introduce bias.

1.1.4 Tracking and Tallying in Time

Because our LO equations will be integrated over the time step, we only need to perform MC tracking for $t \in [t^n, t^{n+1}]$. The initial time for the particle is sampled as described in the previous section. In inverting the **L** operator, particles are tracked until they reach the end of the time step. Path lengths are sampled or the weight is exponentially attenuated as before (e.g., Sec. **??**). As a particle travels from position x_o to x_f, with direction μ, the time is updated as

$$t^f = t^0 + \frac{|x_f - x_o|}{c\mu} \tag{1.9}$$

where c is the speed of light. For analog path-length sampling, if $t^f > t^{n+1}$ then t^f is adjusted to t^{n+1} and the path length is adjusted accordingly. For continuous weight deposition, particles are only tracked until they reach t^{n+1}. A proof that this process of tracking particles is a MC solution to an integral equation that is exactly inverse

to the **L** operator is detailed in [**?**, **?**].

Tallies must be adjusted to account for the averaging over the time step, and to compute the intensity at the end of time step. To produced the time-averaged representation $\overline{I}(x,\mu)$, requires estimators for the average, x, and μ moments of the error, e.g.,

$$\overline{\epsilon}_{x,ij} = \frac{1}{\Delta t}\frac{6}{h_j}\int_{t^n}^{t^{n+1}}\mathrm{d}t\int_{x_{i-1/2}}^{x_{i+1/2}}\mathrm{d}x\int_{\mu_{j-1/2}}^{\mu_{j+1/2}}\mathrm{d}\mu\,\left(\frac{x-x_j}{h_i}\right)\epsilon(x,\mu,t) \tag{1.10}$$

with a similar definition for the average and μ moments. The estimators are defined as

$$\hat{\overline{\epsilon}}_{x,ij} = \frac{1}{N_{hist}}\frac{6}{\Delta t h_i}\sum_{n=1}^{N_{hist}}\frac{s_n}{h_i h_j}w_j\left(x_c - x_i\right), \tag{1.11}$$

where the magnitude of the weights produce the L_1 integral over all phase space, i.e.,

$$\sum_{n=1}^{N} w_n = \|r(x,\mu,t)\|_1 \equiv \int_{t^n}^{t^{n+1}}\mathrm{d}t\int_{x_{i-1/2}}^{x_{i+1/2}}\mathrm{d}x\int_{\mu_{j-1/2}}^{\mu_{j+1/2}}\mathrm{d}\mu\,|r(x,\mu,t)|. \tag{1.12}$$

Here, x_c is the center of the n-th path length, and s_n is the path length for the n-th path length in the $x-\mu$ cell.

Moments of $I^{n+1}(x,\mu)$ must be estimated to represent the end of time step intensity. For example, the x moment for the ij-th cell of the error at the end of time step is

$$\epsilon^{n+1}_{x,ij} = \frac{6}{h_i}\iint_{\mathcal{D}_{ij}}\left(\frac{x-x_i}{h_i}\right)\epsilon(x,\mu,t^{n+1})\mathrm{d}x\mathrm{d}\mu \tag{1.13}$$

The estimators for these moments are a generalization of the census tallies used in IMC [**?**, **?**]. The tallies are based on the definition of the intensity as $I(x,\mu,t) = ch\nu N(x,\mu,t)$ given in Eq. (**??**), similar to collision estimators [**?**, **?**]. The census

estimator for the x moment is

$$\hat{\epsilon}_{x,ij}^{n+1} = \frac{1}{N_{hist}} \frac{6}{h_j h_i} \sum_{n=1}^{N_{hist}} cw_j \left(x_c - x_i\right) \tag{1.14}$$

Similar tallies are defined for the other space-angle moments. These tallies can be exceptionally noisy because only particles that reach the end of the time step contribute.

1.2 Closing the LO Equations in Time

The LO equations must be closed in time consistently with the HO equations. Previous work has enforced consistency in time by adding a local artificial source to the time-discretized LO equations in each cell [**?**]. This source was approximated based on the difference between the exact HO integral of the time derivative and the approximate representation in the LO equations. The advantage of this form is that the LO solver exclusively deals in time-averaged unknowns for the radiation terms in the equations. However, if the problem is strongly non-linear or the time-averaged and time-edge values differ greatly, this may become unstable.

We will alternatively use a parametric closure in the time variable, similar to the spatial closures discussed in the Sec. **??**. The time-integrated LO equations can be written exclusively in terms of time-averaged unknowns. This closure produces LO equations that have the same numerical difficulty to solve as the BE, fully-discrete LO equations, but have the potential to preserve the accuracy of the MC integration in time, upon non-linear convergence of the system. A closure relation is used to eliminate the end of time step moments present from the time derivative term. We will investigate different parametric forms of the closure for robustness. Once the time-averaged unknowns have been calculated, the time closures can be used to convert the time-averaged unknowns to end-of-time-step values.

REWRITE THIS SENTENCE One potential benefit of the time closure parameters is that $\overline{I}^{HO}$ will be most different from $I^{HO,n+1}$ in problems that are optically thin. In such problems, σ_a is small, leading to an optically thin problem. However, there may be difficulties in the MPV problems where the problems are tightly coupled and nonlinear, but can lead to a large change over a time step.

REWRITE: I think most of these paragraphs can be moved to intro

1.2.1 Derivation of Time-Averaged Moment Equations

The time-continuous radiation equations are integrated in space and angle the same as before. For example, the L and $+$ moment equation is

$$\frac{1}{c}\frac{\partial}{\partial t}\langle\phi\rangle_L^+ - 2\left(\mu_{i-1/2}I_{i-1/2}\right)^+ + \langle\mu I\rangle_{L,i}^+ + \langle\mu I\rangle_{R,i}^+ + \sigma_{t,i}h_i\langle\phi\rangle_{L,i}^+ - \frac{\sigma_{s,i}h_i}{2}\left(\langle\phi\rangle_{L,i}^+ + \langle\phi\rangle_{L,i}^-\right) = \frac{h_i}{2}\langle\sigma_a acT^4\rangle_{L,i} \quad (1.15)$$

This equation is then integrated over the time step, and the emission source is assumed implicit. The same manipulations can be performed on the streaming term to form angular consistency terms, but the weighting fluxes are now time-averaged values. Thus, the angular consistency terms are computed with $\overline{I}(x,\mu)$. The equations with time-averaged consistency terms are

$$\frac{\langle\phi\rangle_{L,i}^{+,n+1} - \langle\phi\rangle_{L,i}^{+,n}}{c\Delta t} - 2\overline{\mu}_{i-1/2}^+\overline{\phi}_{i-1/2}^+ + \overline{\{\mu\}}_{L,i}^+\langle\overline{\phi}\rangle_{L,i}^+ + \overline{\{\mu\}}_{R,i}^+\langle\overline{\phi}\rangle_{R,i}^+ + \sigma_{t,i}^{n+1}h_i\langle\overline{\phi}\rangle_{L,i}^{n+1,+} - \frac{\sigma_{s,i}h_i}{2}\left(\langle\overline{\phi}\rangle_{L,i}^+ + \langle\overline{\phi}\rangle_{L,i}^-\right) = \frac{h_i}{2}\langle\sigma_a^{n+1}acT^{n+1,4}\rangle_{L,i}, \quad (1.16)$$

These equations are exact at this point. The BE approximation is used for the temperature terms in the material energy equations, but the radiation energy deposition is a time-averaged valued. REWRITE: Maybe add material energy equation

1.2.2 Parametric Time Closure

The closure relations in time are different than the closure relations for the spatial variable because we do not have a slope in time. The following closure is a modified diamond relation:

$$I^{n+1} = 2\gamma\overline{I} - I^n \tag{1.17}$$

where γ is the closure factor and $\overline{I}$ is the time-averaged intensity. A modified BE discretization can also be used:

$$I^{n+1} = \gamma\overline{I} \tag{1.18}$$

The chosen closure relation must be used to eliminate the unknowns at t^{n+1} from each of the LO moment equations, with the values from the previous time step taken as a known quantity. Thus, it is necessary to have a closure relation for each moment and half range, producing four closure parameters per spatial cell. The closure relations for the L moment and the modified diamond relation are

$$\langle\phi\rangle_{L,i}^{\pm,n+1} = 2\gamma_{L,i}^{\pm}\langle\overline{\phi}\rangle_{L,i}^{\pm} - \langle\phi\rangle_{L,i}^{\pm,n} \tag{1.19}$$

with equivalent definitions for the R moment. Substitution of the above equation into Eq. (1.16)

$$\frac{2}{c\Delta t}\left[\gamma_{L,i}^{+}\langle\phi\rangle_{L}^{+,n+1} - \langle\phi\rangle_{L}^{+,n}\right] - 2\overline{\mu}_{i-1/2}^{+}\overline{\phi}_{i-1/2}^{+} + \overline{\{\mu\}}_{L,i}^{+}\langle\overline{\phi}\rangle_{L,i}^{+} + \overline{\{\mu\}}_{R,i}^{+}\langle\overline{\phi}\rangle_{R,i}^{+} + \sigma_{t,i}^{n+1}h_i\langle\overline{\phi}\rangle_{L,i}^{n+1,+} - \frac{\sigma_{s,i}h_i}{2}\left(\langle\overline{\phi}\rangle_{L,i}^{+} + \langle\overline{\phi}\rangle_{L,i}^{-}\right) = \frac{h_i}{2}\langle\sigma_a^{n+1}acT^{n+1,4}\rangle_{L,i}, \tag{1.20}$$

The other moment equations are analogously defined.

The value of $\gamma_{L,i}^{+}$, $\gamma_{R,i}^{+}$, $\gamma_{L,i}^{-}$, and $\gamma_{R,i}^{-}$ can be computed by substituting the trial-space representation of $I^{HO}(x,\mu,t)$ into Eq. (1.19) and its analogs.

1.3 Computational Results

We will test the HO time closure for several problems that characterize potential physics regime. Throughout this section, for the HOLO method, results that use the backward Euler discretization are indicated with HOLO-BE and the MC-based time closure are indicated with HOLO-TC, where applicable. We will compare sample statistics and accuracy against IMC simulations. The systematic sampling algorithms detailed in Sec. **??** and Sec. 1.1.2 were used for all HOLO results in this section. In the algorithm the average is set to the floor value and slopes to zero in such cells.

1.3.1 Near-Void Problem

For the first problem, the material properties are uniform throughout a 2.0 cm wide domain with $\rho c_v = 0.01374$ Jks cm^{-3} keV^{-1}, $\sigma_a = 10^{-6}$ cm^{-1}, and $\sigma_s = 0$ cm^{-1}. The material and radiation are initially in equilibrium at a temperature of 0.01 keV. An isotropic incident intensity with $T_r = 0.150$ keV is applied at $x = 0$ for $t > 0$; the incident intensity on the right boundary is 0.01 keV. The simulation end time is 0.003 sh. Because the problem is optically thin, no importance sampling on the interior of the time step is used. For this problem, we expect IMC to be accurate because the small opacity leads to the material energy equation being mostly uncoupled.

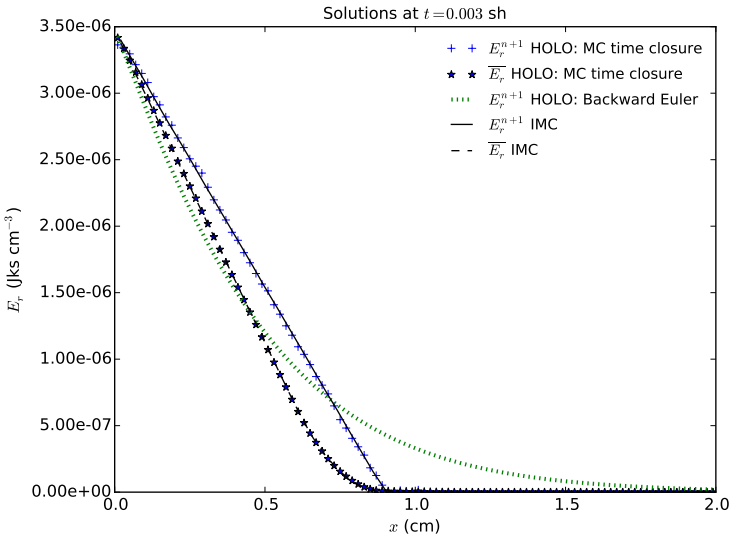

Figure 1.2: Comparison of radiation energy densities of IMC and HOLO method for the HO time closure and a BE discretization.

A comparison of the cell-averaged radiation energy densities E_r for IMC and the HOLO method with the diamond-like HO time closure are depicted in Fig. 1.2, both for the time-averaged solutions and end-of time step values, from the final time step. The end of time step value for the HOLO method with a BE discretization is also depicted. For the HOLO results, three ECMC batches were performed with a total of 3×10^6 histories per time step and the IMC results were generated with 12×10^6 histories per time step. The minimum number of histories for any sampled space-angle cell, N_{cut}??? in Eq. (**??**), is 20 for all HOLO simulations. The spatial meshs had 100 spatial cells and both HOLO results used 20 μ cells. The MC treatment of the time variable and the closure of the LO equations allow the LO results to correctly reconstruct the wave-front location of IMC, whereas the BE discretization artificially propagates energy. Although not plotted, the results were visually equivalent for either the diamond-like or implicit-like closures in this problem. This is because

the problem is nearly linear due to the small opacities, so the HO moments are reproduced accurately, independent of the chosen closure equation.

A comparison of similar results, but plotted as radiation temperatures, is plotted in Fig. **??**. By plotting proportional to the fourth-root of the radiation energy density, the noise at low magnitudes past the wave-front are more apparent in the 3 batches and $\Delta t = 0.001$ case. This noise is small relative to the scale of E_r, but it demonstrates a defficiency of the trial space. The cause is from the step representation over the time step leading to particles sampled near the wave-front with a time near t^n that travel into the equilibrium region. It is noted this is not a bias, but rather an undersampling; if sufficient histories were performed there would be negative particles that canceled out this error. This effect is significantly reduced when a smaller time step is taken, although it increases the projection error between time steps.

For the case of a single batch, there is less noise past the wavefront because the choice of $I^n(x, \mu)$ and an initial guess for $I^{n+1}(x, \mu)$ prevents most particles from traveling past what the physical transport should allow. The discrepancy betweeen the IMC and HOLO solution near the foot of the wave is a result of the spatial discrepancy between the LDFE HO projection and the lumped LD LO equations; this dispersion is not present in the HO solution. This discrepancy can also lead to some negativities in the LD representation of $\phi^{n+1}(x)$, which are set to the floor value for the next calculation.

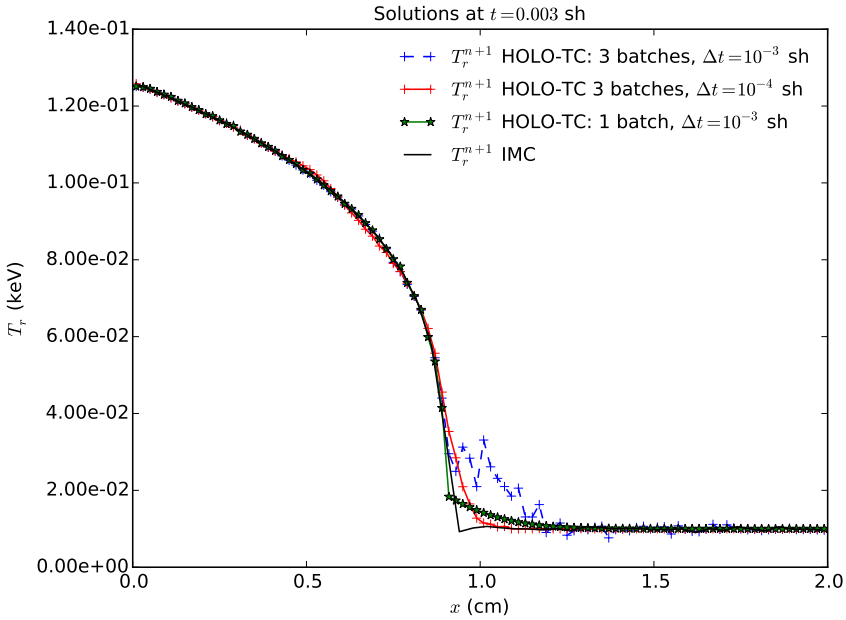

Figure 1.3: Comparison of radiation temperatures of IMC and the HOLO method for different time step sizes and numbers of batches.

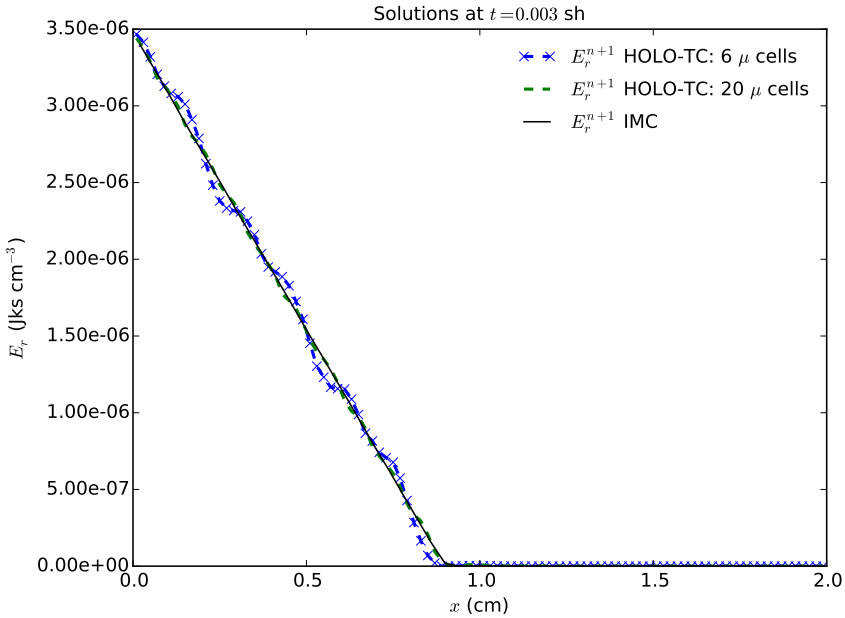

Figure 1.4: Comparison of radiation energy densities for the HOLO method with different numbers of μ cells. $\Delta t = 0.001$ sh

Figure. 1.4 compares radiation energy densities for various numbers of μ cells. At coarser mesh sizes, the imprinting of the mesh is visible in the location of the wave-front. This is a result of the projection onto the space-angle mesh between time steps. As the mesh is refined, the solution converges towards the IMC solution. Smaller time step sizes can increase the mesh imprinting because the projection onto the trial space happens more often. However, it is important to note that the mesh imprinting will be reduced as σ_a is increased and absorption-emission events smooth the angular intensity across each time step.

We have computed FOM statistics using Eq. (**??**) with 20 independent runs for each problem set up and parameters. The statistics are computed based on the time-averaged radiation energy densities. It is noted that the FOM results for each time step size are normalized to the IMC results within that table. The results

are compared for two different time step sizes in Tables 1.1 and 1.2. The different number of batches for the HOLO methods are indicated in parenthesis next to the method names. The results demonstrate that IMC can be more efficient than the ECMC method at longer time step sizes. This is a limiting case; because minimal absorptions are occuring in this problem, the IMC method is just advancing the initially sampled census particles between time steps, so there is negligible resampling of the phase space. Whereas, ECMC must resample the residual source and the step trial-space on the interior of the tiem step has a larger truncation error. At smaller time step sizes, the ECMC method, particularly for the single batch case, becomes more efficient than IMC.

Table 1.1: **Comparison of sample statistics for the time-averaged radiation energy densities, of the last time step, for the near-void problem and $\Delta t = 0.001$ sh. Simulation end time is t = 0.003 sh.**

	$\|s\|$			FOM		
hists./step	IMC	HOLO-TC (1)	HOLO-TC (3)	IMC	HOLO-TC(1)	HOLO-TC(3)
300,000	0.27%	0.27%	0.45%	1.00	0.96	0.35
3,000,000	0.09%	0.06%	0.15%	1.04	2.19	0.33

Table 1.2: **Comparison of sample statistics for the time-averaged radiation energy densities, of the last time step, for the near-void problem and $\Delta t = 10^{-4}$ sh. Simulation end time is t = 0.003 sh.**

	$\|s\|$			FOM		
hists./step	IMC	HOLO-TC (1)	HOLO-TC (3)	IMC	HOLO-TC(1)	HOLO-TC(3)
30,000	2.46%	0.44%	1.65%	1.00	31.07	2.22
300,000	0.80%	0.12%	0.37%	0.95	43.66	4.47

1.4 Optically Thin Problem

We modify the problem in the previous problem by simply increasing the opacity to 0.2 cm^{-1}.

1.5 Mixed Optical Thickness Problem

It is important to demonstrate that the time-continuous case is still efficient in a mix of optically thick and optically thin regions. Simulations are performed for a three region problem detailed in Fig. **??**.

REFERENCES

[1] J.E. Morel, T.A. Wareing, and K. Smith. Linear-Discontinuous Spatial Differencing Scheme for S_n Radiative Transfer Calculations. *Journal of Computational Physics*, 128:445–462, 1996.